

# A local PDE model of aggregation formation in bacterial colonies

Paul-Christopher Chavy-Waddy\* and Theodore Kolokolnikov†

July 14, 2016

## Abstract

We study pattern formation in a model of cyanobacteria motion recently proposed by Galante, Wisen, Bhaya and Levy. By taking a continuum limit of their model, we derive a novel fourth-order nonlinear parabolic PDE equation that governs the behaviour of the model. This PDE is  $u_t = -u_{xx} - u_{xxxx} + \alpha \left( \frac{u_x u_{xx}}{u} \right)_x$ . We then derive the instability thresholds for the onset of pattern formation. We also compute analytically the spatial profiles of the steady state aggregation density. These profiles are shown to be of the form  $\text{sech}^p$  where the exponent  $p$  is related to the parameters of the model. Full numerical simulations give a favorable comparison between the continuum and the underlying discrete system, and show that the aggregation profiles are stable above the critical threshold.

## 1 Introduction

The goal of this paper is to derive a new PDE for a model of bacterial aggregation. In a series of papers [1, 2, 3, 4, 5], the authors proposed several models of motion of cyanobacteria *Synechocystis sp.* Two key aspects are observed experimentally: the formation of aggregates – areas of high bacterial density; and the motion towards light (phototaxis). Phototaxis requires sufficiently high light density to proceed. By contrast, aggregates form even in the absence of light, and they also help with phototaxis when the light gradient is sufficiently high. To understand the formation of aggregates in low light, in papers [4, 5, 3], the authors proposed that it can be a result of quasi-random motion, in agreement with experiments. As observed in [4], “Some cells move in a persistent pattern, in a direction that changes frequently, with no apparent bias towards light.” In [4] the authors proposed a simple stochastic agent-based model which leads to aggregation. In [2], they further refined this model in the simple one-dimensional setting. By averaging out the noise, they obtained an ODE model on a lattice for the average density. They also extended this model to two dimensions in [3].

For reader’s convenience, let us present a simplified derivation of the model in [2] here. Each bacterium is oriented either left or right. At each time-step, the bacterium either moves to an adjacent cell according to its current orientation, or – with a certain rate – it chooses a new orientation and then moves to an adjacent cell. The choice of new orientation is not completely random; rather the bacterium picks at random another bacterium within its sensing radius, and then orients itself to move towards it. In the mean field limit, these assumptions lead to the following ODE model on a lattice consisting of  $n$  bins:

---

\*Department of Mathematics and Statistics, Dalhousie University, Halifax, NS, Canada, B3H 4R2. Email: p1859327@dal.ca.

†Department of Mathematics and Statistics, Dalhousie University, Halifax, NS, Canada, B3H 4R2. Email: tkolokol@gmail.com.

$$\frac{dR_j}{dt} = aR_{j-1} - (a+c)R_j + cU_{j-1}\eta_{j-1}^+ \quad (1a)$$

$$\frac{dL_j}{dt} = aL_{j+1} - (a+c)L_j + cU_{j+1}\eta_{j+1}^- \quad (1b)$$

$$U_j = L_j + R_j; \quad (1c)$$

$$\eta_j^\pm = \frac{\sum_{k=1}^d U_{j\pm k}}{\sum_{k=1}^d (U_{j+k} + U_{j-k})} \quad (1d)$$

Here,  $R_j(t)$  and  $L_j(t)$  is the density of right and left-moving bacterium in the bin  $j = 1 \dots n$  at time  $t$ ;  $a$  is the rate with which the bacterium moves one bin according to its orientation;  $c$  is the rate with which the bacterium moves after switching to a new orientation. The parameter  $d$  is the sensing radius of the bacterium. System (1) is in fact equivalent to a slightly more complicated model presented in [2]<sup>1</sup>

In this paper we provide some insights into the model (1) and derive a new PDE system based on the continuum limit of (1). We start by computing thresholds for the formation of aggregates. In §3, using linear stability analysis of homogeneous steady state, we find that the aggregates form when  $c > c_0$  where  $c_0 = 2a/d$ . By contrast, for  $c < c_0$ , the system converges to a homogeneous solution. Biologically, this indicates that the bacterium must “look around” within its sensing radius and change the orientation accordingly with sufficient frequency in order to be able to form aggregates.

When  $c > c_0$ , to study the shape and extent of the aggregates, in §4 we derive the continuum limit of the the model (1) in the limit of large number of bins. In an appropriate limit, we obtain the following novel parabolic PDE:

$$u_t = -u_{xx} - u_{xxxx} + \alpha \left( \frac{u_x u_{xx}}{u} \right)_x. \quad (2a)$$

Here,  $\alpha$  is given in (20) in terms of model parameters, and it controls the extent of the aggregate. This PDE allows us to give a formula for the profile of the aggregation spike. We show that (2a) admits a steady state solution in the form of a spike, given by

$$u(x, t) = C \left[ \operatorname{sech} \left( \frac{\sqrt{\alpha-1}}{2} x \right) \right]^{\frac{2}{\alpha-1}}. \quad (3)$$

The model (1) is closely related to a larger class of “swarming” models of biological aggregation, based on social attraction-repulsion forces; see for example [6, 7, 8, 9]. Broadly speaking, the two main approaches consist of modeling individuals as particles, resulting in a large ODE system for particle positions, or take the continuum limit of the particle model, which yields a non-local PDE for swarm density and velocity [10, 11, 12, 13, 14]. Recently in [15], the authors considered an aggregation model with non-local repulsion, and used a low-frequency truncation in the Fourier space to approximate the nonlocal PDE by a local fourth-order PDE of Cahn-Hilliard type:  $u_t = (u(u - u^2 - u_{xx}))_x$ . They were also able to construct an inhomogeneous steady state. Their model is related to models used in thin-film models, and the steady state profiles typically have a plateau, with the density having a discontinuous second derivative at the boundary  $u = 0$ .

<sup>1</sup>The system presented in [2] (see equation (17-20) there) has four variables:  $R_i^m$ ,  $L_i^m$ ,  $R_i^s$ ,  $L_i^s$ , corresponding to motile or stationary, and left or right-moving populations. Defining  $R_i = R_i^m + R_i^s$  and  $L_i = L_i^m + L_i^s$ , one then obtains (1) directly from equations (17-20) of [2].

There are also many local models in the literature that exhibit spike solutions such as (3). Most of these are reaction-diffusion systems involving two or more components. This includes the widely-used Keller-Segel model [16] and its many variants [17, 18, 19, 20, 21]; the Gray-Scott model [22] and the Gierer-Meinhardt model [23]. Some other examples of PDE models that exhibit spike patterns include [24, 25, 26, 27]. These models are reaction-diffusion systems involving two or more components, often with nonlocal terms. By contrast, the PDE we derived is a single fourth order equation. This is among the simplest possible settings that give rise to a stable spike solution.

The summary of the paper is as follows. In §2 we rewrite the model (1) in a symmetric form, which is more convenient for analysis. In §3 we derive the stability of the homogeneous state. The continuum (PDE) limit is derived in §4 and we construct the spike profile in §5. We conclude with some open problems in §6.

## 2 Symmetrization

To simplify the subsequent analysis, we first recast the model (1) in a more symmetric form. In particular this step is essential in deriving the continuum limit. Using  $U_j = R_j + L_j$  and adding (1a) and (1b) we obtain

$$\frac{dU_j}{dt} = a(R_{j-1} + L_{j+1}) - (a+c)U_j + c(U_{j-1}\eta_{j-1}^+ + U_{j+1}\eta_{j+1}^-) \quad (4)$$

To obtain a closed system, define

$$V_j = R_{j+1} + L_{j-1}. \quad (5)$$

Note that

$$\frac{dR_{j+1}}{dt} = aR_j - (a+c)R_{j+1} + cU_j\eta_j^+ \quad (6a)$$

$$\frac{dL_{j-1}}{dt} = aL_j - (a+c)L_{j-1} + cU_j\eta_j^- \quad (6b)$$

and recall from (1d) that  $\eta_j^+ + \eta_j^- = 1$ . Adding (6a) and (6b) together we therefore obtain

$$\frac{dV_j}{dt} = (a+c)(U_j - V_j) \quad (7)$$

Finally, rewrite  $R_{j-1} + L_{j+1} = U_{j-1} + U_{j+1} - (L_{j-1} + R_{j+1}) = U_{j-1} + U_{j+1} - V_j$ . In summary, the model (1) is equivalent to

$$\frac{dU_j}{dt} = a(U_{j-1} + U_{j+1} - V_j) - (a+c)U_j + c(U_{j-1}\eta_{j-1}^+ + U_{j+1}\eta_{j+1}^-) \quad (8a)$$

$$\frac{dV_j}{dt} = (a+c)(U_j - V_j) \quad (8b)$$

$$\eta_j^\pm = \frac{\sum_{k=1}^d U_{j\pm k}}{\sum_{k=1}^d (U_{j+k} + U_{j-k})}. \quad (8c)$$

Physically speaking,  $V_j = R_{j+1} + L_{j-1}$  represents the density of bacteria in the immediate vicinity of bin  $j$  that is currently diffusing away from bin  $j$ , whereas  $U_j = R_j + L_j$  is the total density of bacteria. Formulation (8) has the considerable advantage of having the second equation reduce to a simple linear ODE. Moreover, both equations are completely symmetric about the index  $j$ . It turns out that this will be advantageous for many of the calculations we will carry out. As such, this is the formulation we use for the remainder of this paper.

Note that (8b) suggests that  $V_i$  decays towards  $U_i$ . Numerical simulations indicate that this is indeed the case, after an initial transient period. Setting  $V_i = U_i$  in (8a) then yields a simplified model,

$$\frac{dU_j}{dt} = U_{j-1} \left( a + c\eta_{j-1}^+ \right) + U_{j+1} \left( a + c\eta_{j+1}^- \right) - (2a + c)U_j. \quad (9)$$

This system has the following simple interpretation. At each time step, the species moves one lattice spacing at random with rate  $a$ , and it moves one lattice spacing towards itself with rate  $c$ .

### 3 Stability of the constant state

The original model (1) admits a homogeneous equilibrium  $L_j = R_j = C$  for any constant  $C$ . In this section we analyse the stability of this equilibrium. It is more convenient to carry out the analysis for the symmetrized system (8) whose steady state is given by  $U_j = V_j = U$ . We perturb

$$U_j(t) = U + \phi_j(t); \quad V_j(t) = U + \psi_j(t) \quad (10)$$

where  $|\phi_j|, |\psi_j| \ll 1$  and we obtain the linearized equations

$$\begin{aligned} \frac{d\phi_k}{dt} = & \left( a + \frac{c}{2} \right) (\phi_{k-1} + \phi_{k+1}) - a\psi_j - (a + c)\phi_j \\ & + \frac{c}{4d} (2\phi_j + \phi_{j-1} + \phi_{j+1} - \phi_{j+d} - \phi_{j-d} - \phi_{j+d+1} - \phi_{j-d-1}) \end{aligned} \quad (11a)$$

$$\frac{d\psi_j}{dt} = (a + c)(\phi_j - \psi_j). \quad (11b)$$

This  $(2n) \times (2n)$  linear problem is decomposable into  $n$  2x2 subproblems as follows. Make an ansatz

$$\phi_j = \phi e^{\lambda t} e^{\frac{2\pi m j i}{n}}; \quad \psi_j = \psi e^{\lambda t} e^{\frac{2\pi m j i}{n}}; \quad m = 0 \dots n-1$$

to obtain

$$\lambda\phi = (2a + c)\phi \cos(\theta) - a\psi - (a + c)\phi + \frac{c}{2d}\phi(1 + \cos\theta - \cos(d\theta) - \cos((d+1)\theta)) \quad (12a)$$

$$\lambda\psi = (a + c)(\phi - \psi) \quad (12b)$$

where

$$\theta = \frac{2\pi m}{n}; \quad m = 0 \dots n-1. \quad (12c)$$

There are two eigenvalues for each choice of  $m$ , giving  $2n$  eigenvalues in total. The solution of the 2x2 eigenvalue problem (12) is given by a quadratic

$$\lambda^2 - (f(\theta) - c)\lambda - (a + c)f(\theta) = 0 \quad (13)$$

where we defined

$$f(\theta) = (2a + c)(\cos(\theta) - 1) + \frac{c}{2d}(1 + \cos(\theta) - \cos(d\theta) - \cos((d+1)\theta)). \quad (14)$$

Note that  $f(\theta) - c \leq 0$  for all  $\theta$  so that a sufficient and necessary condition for stability is that  $f(\theta) < 0$  for all  $\theta$ . Elementary computations show that the instability first appears at  $\theta = 0$ . Since  $f(0) = f'(0) = 0$ , the threshold is obtained by setting  $f''(0) = -2a + dc = 0$ , which yields

$$c_0 = 2a/d \quad (15)$$

for the critical threshold value; the homogeneous steady state is stable if  $c < c_0$  and is unstable if  $c > c_0$ . Moreover all the high-frequency modes are stable: the highest-frequency mode corresponds to  $\theta = \pi$  which is always stable since  $f(\pi) = -2(2a + c) < 0$ . This suggests that a continuum approach will be useful.

We remark that the eigenvalues of the simplified model (9) are given by  $\lambda = f(\theta)$  with  $\theta$  as in (12c). Hence there is a spectral equivalence of models (?? and (9): one is stable if and only the other is stable.

Figure 3 illustrates the full dynamics of (8) in stable and unstable regimes. In the unstable regime  $c > c_0$  (figure 3a), pattern formation takes place. In the stable regime  $c < c_0$  (figure 3b), arbitrary initial conditions converge to a constant state. We now turn our attention to the pattern formation that occurs in the unstable regime.

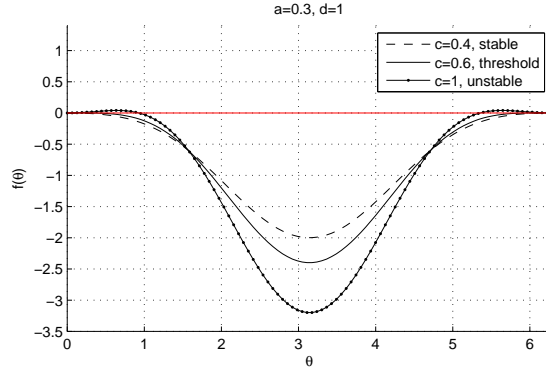


**Figure 1:** The function  $f(\theta)$  given by (14) whose sign determines the stability of the homogeneous steady state. Here,  $d = 1$ ,  $a = 0.3$  and  $c$  is as indicated. It first crosses zero when  $f''(0) = 0$ . The threshold is  $c_0 = 2a/d = 0.6$  with the steady state stable when  $c < c_0$  and unstable when  $c > c_0$ .

## 4 Continuum limit

To study pattern formation which occurs when  $c > c_0$ , we first derive the continuum limit of the bin model (1). Assume that the inter-bin distance is  $h$  and let  $h \rightarrow 0$ . Let  $U_j(t) = u(x, t)$  so that  $U_{j+k}(t) = u(x + kh, t)$  and similarly let  $V_j = v(x, t)$ . We then expand in Taylor series in  $h$ . To simplify the calculation, define

$$g(h) = u(x - h) \frac{\sum_{k=1}^d u(x - h - kh)}{\sum_{k=1}^d u(x - h - kh) + \sum_{k=1}^d u(x - h + kh)},$$

so that the nonlinear terms in the equation (8a) may be written as

$$\begin{aligned} U_{j-1}\eta_{j-1}^+ + U_{j+1}\eta_{j+1}^- &= g(h) + g(-h) \\ &= 2g(0) + h^2 g''(0) + \frac{h^4}{12} g'''(0) + O(h^6). \end{aligned}$$

After some algebra we obtain  $g(0) = \frac{1}{2}u$ ,  $g''(0) = -\frac{d}{2}u_{xx}$  so that up to  $O(h^2)$  terms, we obtain a linear PDE system

$$u_t = a(u - v) - h^2 \left( c \frac{d}{2} - a \right) u_{xx}, \quad v_t = -(a + c)v. \quad (16)$$

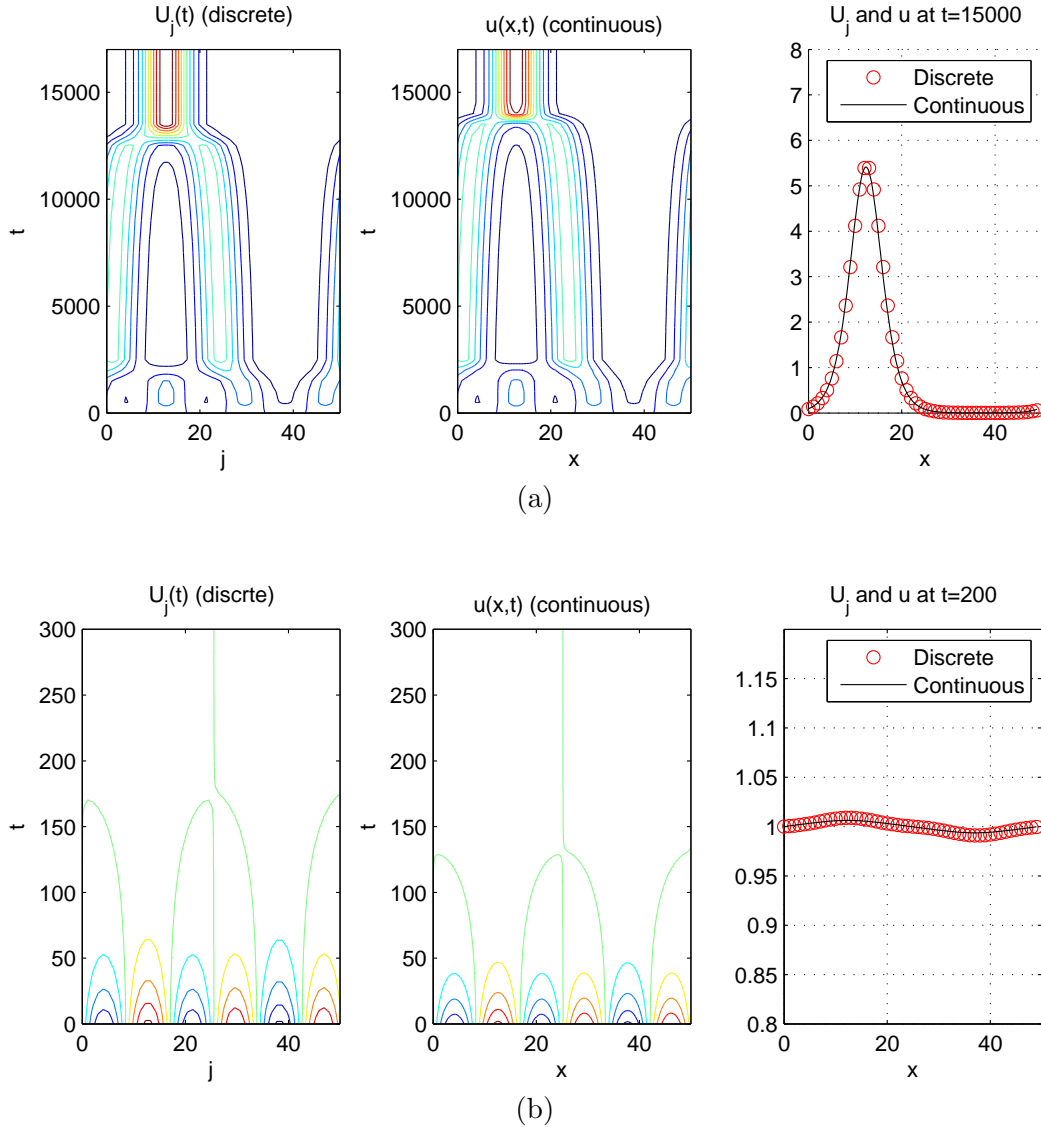


**Figure 2:** Comparison between the discrete model (1) and its continuum limit (18). (a) Left: space-time contour plot of numerical simulation of the discrete model (1) with  $n = 50$ ,  $a = 1$ ,  $c = 2.2$ ,  $d = 1$ . Initial conditions are  $V_j = U_j = 0.01 \sin(2\pi j/n) - 0.2 \sin(6\pi j/n) + 1$ . Middle: space-time plot of continuum model with the same parameters and initial conditions. Right: Comparison of a snapshot at time as indicated. Excellent agreement is observed. Note also the metastable coarsening behaviour which eventually results in a single spike. (b) Same as (a) except with  $c = 1.8$ . The solution converges to a homogeneous steady state.

Linear stability analysis of the homogeneous state  $u(x, t) = v(x, t) = u$  yields the same threshold  $c\frac{d}{2} - a = 0$  as was obtained from the stability analysis of the original discrete system (i.e. equation (15)). Moreover because the system is linear, when  $cd/2 < a$ , the system (16) converges to a constant equilibrium state.

To study the formation of aggregates that happens when  $cd/2 > a$ , we need to incorporate the nonlinear terms which requires an expansion up to  $O(h^4)$ . A very long computation yields

$$g''''(0) = \left[ -\frac{1}{2} - \frac{d}{2} (d^2 + 2d + 3) \right] u_{xxxx} + \frac{(2d+1)(d+1)^2}{2} \left( \frac{u_x u_{xx}}{u} \right)_x \quad (17)$$

and we finally obtain the nonlinear PDE system

$$u_t = a(u - v) - Au_{xx} - Bu_{xxxx} + C \left( \frac{u_x u_{xx}}{u} \right)_x, \quad v_t = (a + c)(u - v); \quad \text{where} \quad (18a)$$

$$A = h^2 \left( c\frac{d}{2} - a \right); \quad B = \frac{h^4}{12} \left( \frac{c}{2} [1 + d(d^2 + 2d + 3)] - a \right); \quad C = \frac{h^4}{24} c(2d+1)(d+1)^2. \quad (18b)$$

This system is a good approximation for parameter values close to the threshold  $c \sim c_0 = ad/2$ . The form of the second equation as well as numerics indicate that, except for an initial transient period,  $v$  quickly approaches  $u$ . Assuming that  $cd/2 > a$  (i.e.  $c > c_0$ , when the homogeneous steady state is unstable), we further reduce (18) to a single dimensionless PDE by setting  $u = v$  and scaling  $x = \hat{x} (B/A)^{1/2}$ ;  $t = \hat{t} BA^{-2}$ . After dropping the hats we then obtain the simplified model

$$u_t = -u_{xx} - u_{xxxx} + \alpha \left( \frac{u_x u_{xx}}{u} \right)_x \quad (19)$$

where

$$\alpha := \frac{c(2d+1)(d+1)^2}{c[1 + d(d^2 + 2d + 3)] - 2a}. \quad (20)$$

With some algebra, it can be shown that  $\alpha > 1$  under the usual assumption  $c > \frac{2a}{d}$  (in fact,  $\alpha > 12/7$ , with this lower bound corresponding to  $d = 1$  and  $c \rightarrow \infty$ ). The condition  $\alpha > 1$  will be important later for deriving the steady state of the system.

Note that the ‘‘backwards-diffusion’’ term  $-u_{xx}$  in (19) has a destabilizing effect, but it is balanced by the fourth-order term  $-u_{xxxx}$  which stabilizes the high-frequency modes. As will be shown in §5, the nonlinear term in the equation is responsible for the formation of stable aggregation patterns.

Figure 2 shows a direct comparison between the discrete system (8) and the continuum limit (18). For the simulation of the continuous system, we used finite differences with a semi-implicit stepping on the  $u$  equation, and forward-Euler stepping on the  $v$  equation. That is, we discretize the space so that  $u(x, t) \sim \vec{u}(t)$  where  $\vec{u}$  is the discretized vector approximation for  $u$  and similarly for  $v$ , and discretize the PDE as

$$\frac{\vec{u}(t + \Delta t) - \vec{u}(t)}{dt} = a(\vec{u}(t) - \vec{v}(t)) - AL_2\vec{u}(t + \Delta t) - BL_4\vec{u}(t + \Delta t) + CL_1 \left( \frac{L_1\vec{u}L_2\vec{u}}{\vec{u}} \right), \quad (21a)$$

$$\frac{\vec{v}(t + \Delta t) - \vec{v}(t)}{dt} = (a + c)(\vec{u}(t) - \vec{v}(t)). \quad (21b)$$

The operators  $L_i$  denote the discretization of the  $i$ th derivative. We used centered differences for  $L_1$  and  $L_2$ , and used  $L_4 = (L_2)^2$ . In the simulations of figure 3, we used 150 meshpoints for the continuous model with  $dt = 0.1$  for both discrete and continuum models. As the simulations show, there is an excellent agreement between the two models.

In agreement with the linear theory, the system converges to a constant state when  $c < c_0$ . On the other hand, when  $c > c_0$ , a complex pattern formation mechanism is observed: several spikes form, followed by a slow coarsening process, until only a single spike remains. In the next section we construct the profile of such a spike.

## 5 Inhomogeneous steady state

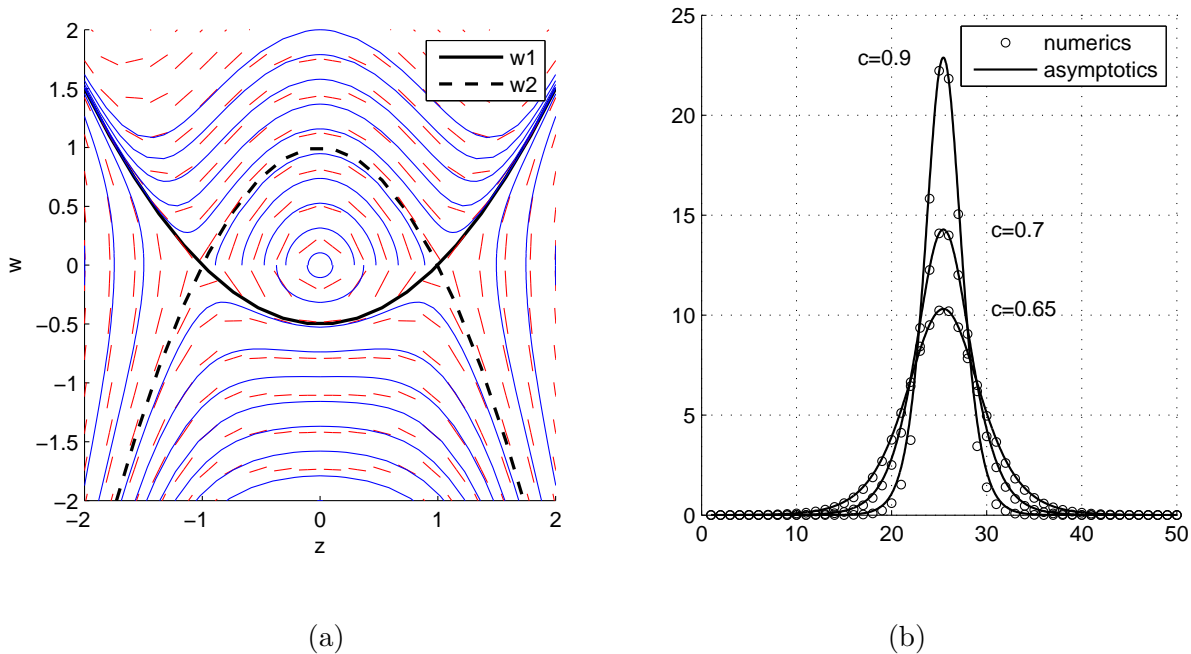


**Figure 3:** (a) Vector field corresponding to (24). Special orbits  $w_1, w_2$  are indicated. They correspond to homoclinic connections between the equilibria  $(z, w) = (\pm\sqrt{\alpha-1}, 0)$ . (b) Comparison between the aggregate steady state of (8) and asymptotics (27). Parameter values are  $n = 50$ ,  $a = 0.3, d = 1$  and with  $c$  as indicated.

We now consider the inhomogeneous steady state on an infinite line when  $c > c_0$ . We set  $u_t = 0$  in (19) and integrate once. Assuming that  $u(x) \rightarrow 0$  as  $x \rightarrow \pm\infty$ , the constant of integration is zero and the steady state then satisfies

$$0 = -u_x - u_{xxx} + \alpha \frac{u_x u_{xx}}{u}. \quad (22a)$$

Equation (22a) has an interesting special closed-form solution, which we will now derive. The ODE (22a) admits a scaling symmetry  $u \rightarrow \lambda u$  which suggests a change of variables  $u = \exp(v)$ . This transforms the scaling symmetry into a translational symmetry and therefore yields a reduction of order by letting  $v_x = z$ :

$$z'' + z + (3 - \alpha)zz' + (1 - \alpha)z^3 = 0, \quad z = u_x/u. \quad (23)$$

Rewrite (23) as a first-order system

$$\frac{dz}{dx} = w; \tag{24a}$$

$$\frac{dw}{dx} = -z + (\alpha - 3)zw + (1 - \alpha)z^3. \tag{24b}$$

The phase portrait of this system is shown in figure 3(a), with heteroclinic orbits connecting the two saddles indicated. The orbits of this system satisfy a first order Abel ODE:

$$\frac{dw}{dz} = \frac{-z}{w} - (3 - \alpha)z - (1 - \alpha)\frac{z^3}{w}. \tag{25}$$

It turns out that the heteroclinic orbits have a particularly simple form:  $w = Az^2 + B$ . Substituting this ansatz back into (25) we obtain two possible solutions

$$w_1 = \frac{(\alpha - 1)z^2 - 1}{2}; \quad w_2 = -z^2 + \frac{1}{\alpha - 1}.$$

If  $w = w_1$  then (24a) yields

$$\frac{dz}{dx} = \frac{(\alpha - 1)z^2 - 1}{2} \tag{26}$$

so that

$$v'(x) = z = -(\alpha - 1)^{-1/2} \tanh\left(\frac{(\alpha - 1)^{1/2}}{2}x\right)$$

and using  $u = \exp(v)$  we finally obtain the profile of the steady state,

$$u(x) = C \left[ \operatorname{sech}\left(\frac{\sqrt{\alpha - 1}}{2}x\right) \right]^{\frac{2}{\alpha - 1}}. \tag{27}$$

On the other hand, if  $w = w_2$  we obtain  $u = C \cosh\left((\alpha - 1)^{-1/2}x\right)$  which is unphysical, since it blows up for large  $x$ .

In figure 3(b) we show a direct comparison between the inhomogeneous steady state of the discretized model (1) (shown in circles) and the continuum-limit approximation (27) (shown using solid line). The circles were obtained using time-integration of (1), until it converged to a single-spike steady state. The normalizing constant  $C$  in (27) was chosen so that  $u(x)$  has the same mass as the discrete solution.

While our construction assumed an infinite domain, numerics indicate that a spike solution exists on a finite domain (with either periodic or Neumann boundary conditions), as long as the domain is sufficiently large (see figure 3(b)). By periodic extension, this implies the existence of  $K$ -spike solutions on a domain of  $K$  times the size.

Several profiles are compared for different values of  $c$ ; good agreement is observed. Note however that the agreement is better when  $c$  is closer to  $c_0 = 0.6$ ; this is in agreement with the formal asymptotics which in principle assume that  $c$  is close to  $c_0$ , although in practice the approximation appears to work well as long as the width of the spike spans enough grid points.

## 6 Discussion

In this paper we investigated the stability properties of the lattice model (1) introduced in [2], derived the continuum limit approximation resulting in a PDE, and computed analytically the aggregation spike profile.

The lattice model (1) incorporates particle direction information. It is very closely related to the simpler model (9) which does not have direction information. The latter is one of the simplest possible models of particle aggregation.

We only scratched the surface for the PDE model (19). The stability of spike solutions remains an open problem. For a single spike on entire line, the stability problem is obtained by linearizing  $u(x, t) = u_0(x) + e^{\lambda t} \phi(x)$ , resulting in the following problem:

$$\lambda \phi = -\phi_{xx} - \phi_{xxxx} + \alpha \frac{\partial}{\partial x} \left( \frac{u'_0}{u_0} \phi_{xx} + \frac{u''_0}{u_0} \phi_x - \frac{u''_0 u'_0}{u_0^2} \phi \right). \quad (28)$$

Here,  $u_0(x)$  is given by (27). Numerical computations of the problem (28) suggest that all eigenvalues are negative, in agreement with the full numerical simulation of (19), as well as the original lattice model (1). Moreover, these computations also suggest that there is a continuous spectrum along the negative real axis the  $\lambda < 0$ .

For simplicity, as a first step we only considered a one-dimensional model in this paper. It is an important open problem to extend this work to two dimensions. Two dimensional motion is complicated by the fact that the direction angle is an additional independent variable. A possible simplifying assumption is to restrict the motion along four directions (west-right-north-south) [3]. However this assumption introduces artefacts which are undesirable, such as concentrations on curves [3]. It is an open problem to derive the continuum limit in two dimensions.

Another future project is to incorporate proliferation mechanisms, such as logistic growth. It would be interesting to see if incorporating such a mechanism can lead to the formation of multiple spikes or more complex dynamics. For instance in [19], very complicated dynamics were observed when adding logistic growth to a well-known Keller-Segel chemotaxis model.

Numerically, we observed metastable behaviour for a solution that consists of two or more spikes (see figure 2), whereby two spikes eventually collide after a very long time, suggesting an instability due to (possibly exponentially small) translational eigenvalues. Similar metastability is observed in Cahn-Hilliard PDE, see for example [28, 29]. A single spike solution, on the other hand, appears to be stable.

Phototaxis effects can be incorporated into the model, for example by modifying the expressions for the transition probabilities  $\eta^\pm$  in (1d). Finally, in [3], Weinberg and Levy generalize the model to two dimensions by considering particles moving in four directions on a square lattice rather than two directions on a binned line. It would be interesting to see which of our results can be generalized to two spatial dimensions.

## References

- [1] Levy, D. L & Requeijo, T. (2008) Stochastic models for phototaxis. *Bulletin of Mathematical Biology* **70**, 1684–1706.
- [2] Galante, A & Levy, D. (2013) Modelling selective local interaction with memory. *Physica D* **260**, 176–190.

- [3] Weinberg, D & Levy, D. (2014) Modelling selective local interaction with memory: Motion on a 2d lattice. *Physica D* **278-279**, 13–30.
- [4] Galante, A, Wisen, S, Bhaya, D, & Levy, D. (2011) Stochastic models and simulations of phototaxis. *Unifying Themes in Complex Systems* **8**, 105–119.
- [5] Galante, A, Wisen, S, Bhaya, D, & Levy, D. (2012) Modelling local interactions during the motion of cyanobacteria. *Journal of Theoretical Biology* **309**, 147–158.
- [6] Cucker, F & Smale, S. (2007) Emergent behaviour in flocks. *IEEE Transactions on Automatic Control* **52**, 852–862.
- [7] Toner, J & Tu, Y. (1998) Flocks, herds and schools: A quantitative theory of flocking. *Physical Review E* **58**, 4828–4858.
- [8] Mogliner, A, Edelstein-Keshet, L, Bent, L, & Spiros, A. (2003) Mutual interactions, potentials, and individual distance in social aggregation. *Journal of mathematical biology* **47**, 353–389.
- [9] Couzin, I. D, Krause, J, James, R, Ruxton, G. D, & Franks, N. R. (2002) Collective memory and spatial sorting in animal groups. *Journal of Theoretical Biology* **218**, 1–11.
- [10] Topaz, C. M & Bertozzi, A. (2004) Swarming patterns in a two dimensional kinematic model for biological groups. *SIAM Journal on Applied Mathematics* **65**, 152–174.
- [11] Topaz, C. M, Bertozzi, A. L, & Lewis, M. E. (2006) A nonlocal continuum model for biological aggregations. *Bulletin of Mathematical Biology* **68**, 1601–1623.
- [12] Fetecau, R. C, Huang, Y, & Kolokolnikov, T. (2011) Swarm dynamics and equilibria for a non-local aggregation model. *Nonlinearity* **24**, 2681.
- [13] Tsimring, L, Levine, H, Aranson, I, Ben-Jacob, E, Schochet, I. C. O, & Reynolds, W. N. (1995) Aggregation patterns in stressed bacteria. *Physical Review Letters* **75**, 1859–1862.
- [14] Mecholsky, N. A, Ott, E, Jr., T. M. A, & Guzdar, P. (2012) Continuum modeling of the equilibrium and stability of animal flocks. *Physica D : Nonlinear Phenomena* **241**, 472–480.
- [15] Bernoff, A. J & Topaz, C. M. (2015) Biological aggregation driven by social and environmental factors: A nonlocal model and its degenerate cahn-hilliard approximation. *arXiv preprint arXiv:1507.04259*.
- [16] Keller, E. F & Segel, L. A. (1971) Model for chemotaxis. *Journal of Theoretical Biology* **30**, 225–234.
- [17] Woodward, D, Tyson, R, Myerscough, M, Murray, J, Budrene, E, & Berg, H. (1995) Spatio-temporal patterns generated by salmonella typhimurium. *Biophysical journal* **68**, 2181.
- [18] Tyson, R, Lubkin, S, & Murray, J. D. (1999) A minimal mechanism for bacterial pattern formation. *Proceedings of the Royal Society of London B: Biological Sciences* **266**, 299–304.
- [19] Wang, Z & Hillen, T. (2007) Classical solutions and pattern formation for a volume filling chemotaxis model. *Chaos: An Interdisciplinary Journal of Nonlinear Science* **17**, 037108.
- [20] Oster, G. F & Murray, J. D. (1989) Pattern formation models and developmental constraints. *Journal of Experimental Zoology* **251**, 186–202.

- [21] Maini, P, Myerscough, M, Winter, K, & Murray, J. (1991) Bifurcating spatially heterogeneous solutions in a chemotaxis model for biological pattern generation. *Bulletin of mathematical biology* **53**, 701–719.
- [22] Pearson, J. E. (1993) Complex patterns in a simple system. *Science* **261**, 189–192.
- [23] Iron, D, Ward, M. J, & Wei, J. (2001) The stability of spike solutions to the one-dimensional gierer–meinhardt model. *Physica D: Nonlinear Phenomena* **150**, 25–62.
- [24] Deroulers, C, Aubert, M, Badoual, M, & Grammaticos, B. (2009) Modeling tumor cell migration: from microscopic to macroscopic. *Physical Review E* **79**.
- [25] Murray, P. J, Edwards, C. M, Tindall, M. J, & Aini, P. K. (2009) From a discrete to continuum model of cell dynamics in one dimension. *Physical Review E* **80**.
- [26] Horstmann, D, Painter, K. J, & Othmer, H. G. (2004) Aggregation under local reinforcement : From lattice to continuum. *European Journal of Applied Mathematics* **15**, 545–576.
- [27] Baker, R. E, Yates, C. A, & Erban, R. (2010) From microscopic to macroscopic descriptions of cell migrations on growing domains. *Bulletin of Mathematical Biology* **72**, 719–762.
- [28] Reyna, L. G & Ward, M. J. (1995) Metastable internal layer dynamics for the viscous cahn-hilliard equation. *Methods and Applications of Analysis* **2**, 285–306.
- [29] Alikakos, N, Bates, P. W, & Fusco, G. (1991) Slow motion for the cahn-hilliard equation in one space dimension. *Journal of differential equations* **90**, 81–135.